J Mater Sci: Mater Electron (2023) 34:391

Structural and magnetic properties of NiCuZn ferrite films deposited using sputtering

Roni Paul[1], Sushma Kotru[1,*], and Jaber A. Abu Qahouq[1]

[1] *Department of Electrical and Computer Engineering, The University of Alabama, Tuscaloosa, AL 35487, USA*

Received: 2 September 2022
Accepted: 28 December 2022
Published online: 4 February 2023

ABSTRACT

Ferrite films are promising materials for power inductor applications. In this work, we investigated the structural and magnetic properties of $Ni_{0.35}Cu_{0.2}Zn_{0.45}Fe_2O_4$ films to understand the correlation between annealing temperature, grain size, crystallite size, lattice constant, microstrain, dislocation density, and magnetic properties. The films were deposited at room temperature on Si substrates using sputtering method. Films were annealed post-deposition to tune the microstructure. The crystallinity and spinel structure of the films were confirmed by x-ray diffraction (XRD) analysis. Scanning electron microscopy revealed that films were crack-free, and a linear growth in the grain size with an increase in annealing temperature was observed. The crystallite size, lattice constant, microstrain, and dislocation density calculated from the XRD data indicate that the lattice imperfection decreased when films were annealed at higher temperatures, resulting in an increase in the value of saturation magnetization. Crack-free films with maximum saturation magnetization of 387 emu/cc were obtained from the film annealed at 800 °C.

1 Introduction

Nickle copper zinc (NiCuZn) ferrite find applications in multilayer chip inductor, low temperature co-fired ceramic (LTCC), electromagnetic shielding sheet, ferrite core, etc., owing to their high resistivity, low eddy current losses, high permeability, high saturation magnetization, and chemical stability [1–6]. NiCuZn ferrite films are being considered for applications such as power inductors, noise suppressors, and radio frequency-integrated inductors [7, 8]. Though there is a large body of literature available for NiCuZn bulk, much work has not been reported for the films of NiCuZn. There are many challenges associated with integrating these films with Si, large-area deposition, and obtaining good magnetic properties from the films.

Recently, NiCuZn ferrite films of varying compositions where Ni = 0.2–0.55, Cu = 0.1–0.2, and Zn = 0.25–0.6 have been prepared using different deposition techniques [9–12]. The fabrication processes used for preparing ferrite films and post-growth annealing temperatures are seen to greatly influence the resulting magnetic properties. Fang et al. prepared $(Ni_{0.2}Cu_{0.2}Zn_{0.6}O)_{1.03}$ $(Fe_2O_3)_{0.97}$/PDMS composite films using the solid-state reaction method, which

Address correspondence to E-mail: skotru@eng.ua.edu

https://doi.org/10.1007/s10854-022-09803-4

resulted in saturation magnetization of 61.77 emu/g [10]. Liu et al. used spin coating method to deposit the films and achieved saturation magnetization of 252.5 emu/cc from $Ni_{0.3}Cu_{0.1}Zn_{0.6}Fe_2O_4$ films annealed at 650 °C [11]. Feng et al. studied $Ni_{0.8-x}Cu_{0.2}Zn_xFe_2O_4$ thin films deposited by sol–gel method and observed a maximum saturation magnetization value of about 271.56 emu/cc for x = 0.45 when the film was calcined at 600 °C [12]. Gao et al. reported a saturation magnetization value of 300 emu/cc from the $Ni_{0.4}Cu_{0.2}Zn_{0.4}Fe_2O_4$ films annealed at 800 °C [13]. Lee et al. used DC sputtering to deposit $Ni_{0.5}Cu_{0.2}Zn_{0.3}Fe_2O_4$ films and obtained saturation magnetization of 262 emu/cc from the films annealed at 800 °C [9].

These results suggest that high annealing temperatures are required to achieve high values of saturation magnetization from these films. However, annealing temperatures of 800 °C and higher have been reported to result in unwanted phases, such as SiO_2 and $FeSiO_3$, and formation of cracks [14, 15]. In our previous work, we investigated $Ni_{0.35}Cu_{0.2}Zn_{0.45}Fe_2O_4$ films prepared by sol–gel method and achieved saturation magnetization of 261 emu/cc after annealing the film at 600 °C [16]. Further annealing at 700 °C or higher temperatures resulted in cracks in the films and degradation of saturation magnetization. This can be attributed to high stress and low density of the films prepared using the sol–gel process. To investigate this further, we used RF sputtering to deposit $Ni_{0.35}Cu_{0.2}Zn_{0.45}Fe_2O_4$ (hereafter referred to as NCuZF) films on Si substrate. The sputtering technique is known for obtaining large-area deposition, high adhesion, homogeneous element distribution, and dense films [17–19]. In general, process parameters during growth, such as sputtering pressure [15, 20], oxygen pressure [21, 22], and sputtering power [23, 24] as well as post-growth parameters such as annealing temperature [16, 25, 26], annealing time [9, 13, 27], and annealing/cooling rate [27, 28] have been reported to play a significant role in the magnetic properties. In this work, we report structural and magnetic properties of NiCuZn ferrite films deposited on Si substrate using sputtering. Crack free films with a high value of maximum saturation magnetization of 387 emu/cc was achieved from these films, which, to the best of our knowledge, is the highest reported value so far.

2 Experimental

A ceramic target of $Ni_{0.35}Cu_{0.2}Zn_{0.45}Fe_2O_4$ composition (obtained from Toshima Manufacturing Co. Ltd.) with a diameter of 2 inch and thickness of 0.125 inch was used for the deposition. Films of NCuZF were deposited on Si (100) substrates using RF sputtering. The base pressure of the chamber was 2×10^{-7} torr. High-purity gases (Ar ~ 12.5 and O_2 ~ 0.5 sccm) were used to maintain the background pressure. RF power of 100 W was used for the deposition of all films. The deposition was carried out at room temperature, and the as-deposited films were annealed at four temperatures (500, 600, 700, and 800 °C) for 10 min using a rapid thermal annealing process. Annealing was carried out in an oxygen environment using a flow rate of 2000 sccm.

The structural properties of the NCuZF films were characterized by X-ray diffractometer (XRD) and field emission scanning electron microscope (FESEM). XRD was conducted with a Bruker D8 discover unit using Co K_α radiation. Surface morphology was obtained using Apreo FESEM. Energy-dispersive spectroscopy (EDS) was used to obtain the elemental distribution of NCuZF films. Magnetic properties of NCuZF films were measured using a vibrating sample magnetometer (VSM). The film thickness was measured using Dektak profilometer. All measurements were taken at room temperature.

3 Results and discussion

3.1 Structural properties

Figure 1 shows XRD pattern for the NCuZF as deposited film and films post-annealed at 500, 600, 700, and 800 °C. The as-grown films were amorphous and post-growth annealing helped in introducing crystallinity in the films. The intensity of films annealed at 500 °C was low as compared to the films annealed at higher temperatures. All films showed peaks attributed to the (111), (220), (311), (222), (400), (422), (511), and (440) planes. The presence of these peaks confirms the formation of cubic spinel structure and the absence of any intermediate phases, which is in agreement with the reported literature for other compositions of NiCuZn ferrite [29]. It was observed that the peaks shifted slightly to higher angle with the higher annealing temperature. For this

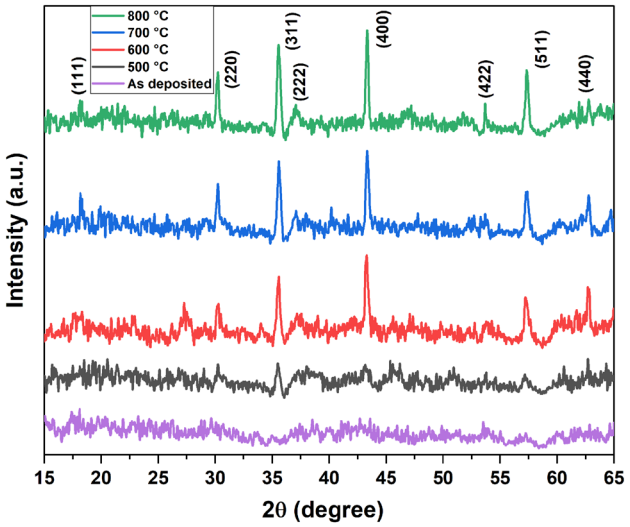

Fig. 1 XRD pattern for the NCuZF as-deposited and post-annealed films, where annealing was done at 500, 600, 700, and 800 °C

work, ICDD-04-020-7944 for $Ni_{0.6}Cu_{0.1}Zn_{0.34}Fe_{1.92}O_{0.92}$ composition was used for indexing the peaks.

The XRD data were used to calculate the crystallite size (D) [30], lattice constant (a) [31], microstrain (ε) [32], and dislocation density (δ) [33] using the following equations:

$$D = \frac{K\lambda}{\beta\cos\theta}$$

$$a = \frac{\lambda}{2\sin\theta}\sqrt{h^2 + k^2 + l^2}$$

$$\varepsilon = \frac{\beta\cot\theta}{4}$$

$$\delta = \frac{n}{D^2}$$

where λ is the wavelength of the X-ray (in nanometers), β is the full width of the diffraction peak at half the maximum intensity (FWHM in radians), K is a constant related to crystalline shape (K = 0.9 used for this work),θ is the Bragg's angle (in radian or degree), (hkl) are the miller indices of planes, and n = 1 (which gives the minimum dislocation density).

Peaks of (400) plane from films annealed at 500, 600, 700, and 800 °C were used for fitting the data to obtain FWHM and for calculating the crystallite size, lattice constant, microstrain, and dislocation density. The calculated values of crystallite size, lattice constant, microstrain, and dislocation density along with the data used for peak analysis are presented in Table 1. Crystallite size of ~ 15.5–34 nm was obtained for films annealed at 500–800 °C which confirms the nanocrystalline formation of NCuZF films. The crystallite size was seen to increase with annealing temperature. Further, the microstrain and dislocation density were observed to decrease with annealing temperature, which is an indication of a decrease in lattice imperfection. This could be due to the reduction of grain boundaries as the crystallite size increased [32]. A slight decrease in the lattice parameter with annealing temperature was also observed for these films, which could be attributed to the cation distribution between tetrahedral and octahedral sites [34]. The cation distribution was drawn using VESTA software and the crystal structure of NCuZF is presented in Fig. 2, where Zn^{2+} occupies A site (tetrahedral), Ni^{2+} and Cu^{2+} occupy B site (octahedral), and Fe^{3+} can move either site.

To further understand the surface morphology of these films, FESEM images were recorded. Figure 3(a–c) represents the FESEM images of the films annealed at 600, 700, and 800 °C. The grain size of films deposited at RT and annealed at 500 °C could not be measured as the grains for these films were not well developed, whereas well-developed grains were observed from the films annealed at 600, 700, and 800 °C. The grain size was obtained by measuring the diameter of individual grains using the line parameter in FESEM. The grain size values presented in Table 2 were obtained by averaging the measurements of ~ 20 grains. A linear increase in the grain size with an increase in annealing temperature was observed. Smaller grains have higher surface energy compared to larger grains. As a result, smaller grains diffuse to larger grains to minimize the total energy. Consequently, larger grains become larger and smaller grains become smaller and even vanish[14]. No cracks were observed in these films.

Figure 4(a–d) represents the EDS spectrum of the films annealed at 500, 600, 700, and 800 °C. The spectrum shows the presence of Fe, Ni, Cu, and Zn, which are the main constituents of NCuZF. The atomic ratio of Ni, Zn, Cu, and Fe calculated from these EDS spectra did not show a significant variation with respect to change in annealing temperature

3.2 Magnetic properties

Figure 5 shows the magnetization as a function of applied field for NCuZF films annealed at 500, 600, 700, and 800 °C. All the magnetization curves

Table 1 Peak Analysis of X-ray diffraction data and calculated values of crystallite size, lattice constant, microstrain, and dislocation density

Sample	2θ (°)	Height (counts)	FWHM (β)	Highest peak (counts)	Crystallite size (D) (nm)	Lattice parameter (Å)	Micro strain (10^{-3})	Dislocation density (10^{15} lines/m^2)
500 °C	43.196	7	0.55	(311) 9	15.51	8.367	6.07	4.16
600 °C	43.284	40	0.34	(400) 40	25.1	8.351	3.74	1.59
700 °C	43.32	41	0.301	(400) 41	27.87	8.345	3.31	1.29
800 °C	43.33	50	0.251	(400) 50	34.04	8.342	2.76	0.86

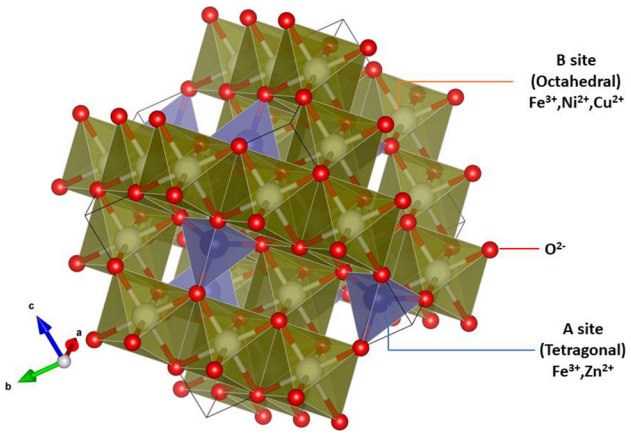

Fig. 2 Crystal structure of NCuZF film

exhibited "S-shape" hysteresis loop which is a typical characteristic of ferrimagnetic materials. The saturation magnetization values of NCuZF films annealed at four different temperatures are summarized in Table 2. The saturation magnetization (M_s) of 219 emu/cc was obtained from the film annealed at 500 °C. A significant change in saturation magnetization was observed for the film annealed at 600 °C, with the saturation magnetization increasing from 219 emu/cc to 317 emu/cc (~ 45% change). Further increase in saturation magnetization was observed from films annealed at higher temperatures. A maximum saturation magnetization of 387 emu/cc was obtained from the film annealed at 800 °C (~ 77% change from 500 °C annealed film). Kancharla et al. obtained saturation magnetization of 139 emu/cc for $CoFe_2O_4$ films which were annealed at 500 °C[35]. Regmi et al. reported saturation magnetization of 290 emu/cc for $NiFe_2O_4$ film deposited at 650 °C[36]. Pradhan et al. achieved saturation magnetization of 363 emu/cc from $Ni_{0.65}Zn_{0.35}Fe_2O_4$ films deposited at 800 °C[37].

As observed from the XRD results, the films annealed at 500 °C were not highly crystalline, whereas films annealed at temperatures above 500 °C resulted in better crystallinity. This could be one of the factors why lower values of magnetization were obtained from films annealed at 500 °C. The increase in saturation magnetization with annealing temperature can also be attributed to the change in grain size. Films annealing at higher temperatures resulted in larger grains compared to those annealed at lower temperatures. When the grain size increases, domain walls are formed. The movement of these domain walls under a magnetic field can also be attributed to the increased magnetization [38]. Moreover, magnetization in ferrites depends on the occupancy of metal ions in their preferred sites. For NCuZF, Ni^{2+} and Cu^{2+} have a preference for the octahedral site and Zn^{2+} has a preference for the tetrahedral site whereas Fe^{3+} can move from an octahedral to tetrahedral site. However, at lower annealing temperatures, Zn^{2+} can occupy the tetrahedral site, thus resulting in lower magnetization. Higher annealing temperatures can help metal cations to be distributed in preferred sites (tetrahedral) resulting in an increase in the magnetization value [38–40]. The saturation magnetization (M_s) is inversely proportional to lattice parameter [27]. Further, from the data of Table 1, the lattice parameter is observed to decrease from 8.367 to 8.342 when the annealing temperature increased from 500 to 800 °C. This decrease in lattice constant values with increase in annealing temperature is also reflected in the saturation magnetization.

The coercivity values obtained from the magnetization data presented in Fig. 5 are summarized in Table 2. The coercivity of the films increased with the increase in grain size until a critical grain size was reached. In magnetic films, grains smaller than critical grain size act as a single domain, defined as a group of magnetic spins oriented in the same

Table 2 Structural and magnetic properties of NCuZF films annealed at 500, 600, 700, and 800 °C

Annealing temperature (°C)	Grain size (nm)	Saturation magnetization (emu/cc)	Coercivity (Oe)
500	na	219	23.5
600	25.9	317	59
700	45.65	342	98
800	58	387	97

direction [41]. The magnetic stability of a single domain gets affected by thermal energy. When the grain size is smaller, thermal agitation is smaller, resulting in fewer fluctuations in the magnetic spin orientations. Therefore, films with smaller grains showed lower coercivity, and films with larger grains showed higher coercivity. On the other hand, grains that are larger than the critical grain size act as multi-domain, and a weak magnetic field can shift domain walls easily in a multi-domain grain resulting in a reduction of coercivity [41, 42]. An increase in the coercivity value was observed until the grain size reached 45.65 nm and coercivity value decreased when the grain size reached 58 nm. From the results, it can be concluded that the critical grain size for the transition of single domain to multi-domain is between 45.65 and 58 nm. Murali et al. calculated the critical grain size value of a single domain to be 50.2 nm for NiZn ferrite, which is in the range reported by authors for NCuZF films prepared using sol–gel [42].

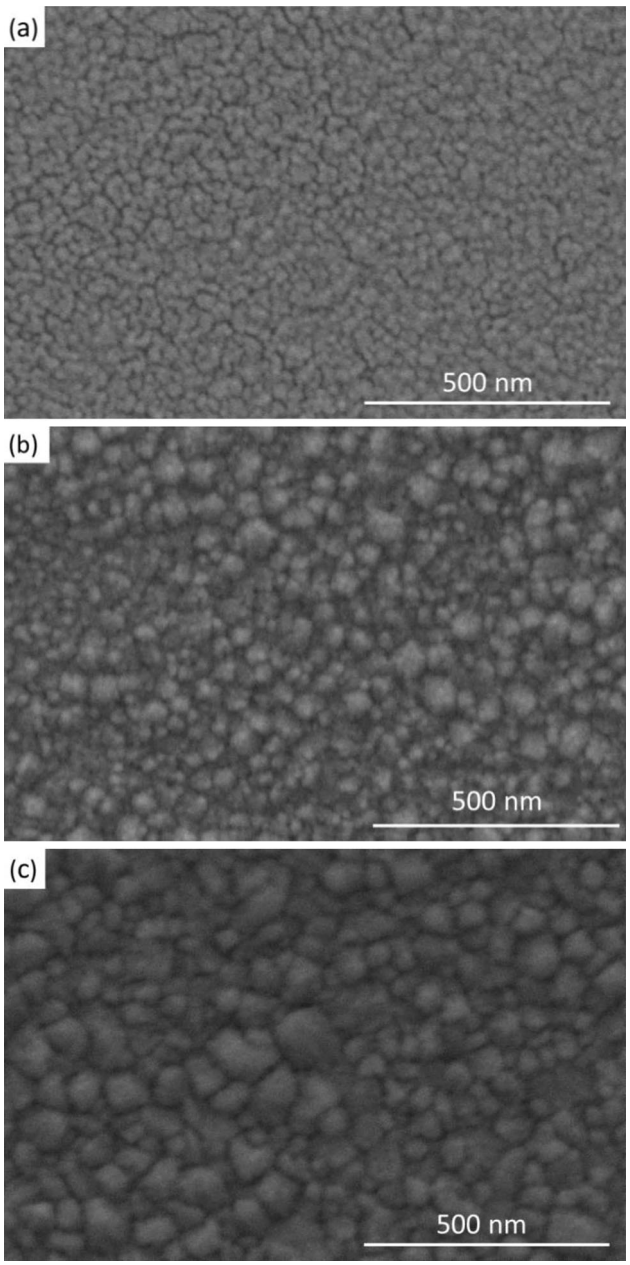

Fig. 3 FESEM images of NCuZF films annealed at different temperatures: **a** 600, **b** 700, and **c** 800 °C

4 Conclusions

$Ni_{0.35}Cu_{0.2}Zn_{0.45}Fe_2O_4$ films were successfully deposited using RF sputtering. The grain size of the films was seen to increase with annealing temperature, whereas the microstrain and dislocation density were observed to decrease with annealing temperature. The saturation magnetization (M_s) of the films increased with the annealing temperature, which is attributed to the larger grains present in those films. The results indicate that the lattice imperfection decreased when films were annealed at a higher temperature, which helped in obtaining the high value of saturation magnetization. The highest saturation magnetization value of 387 emu/cc was obtained for the film annealed at 800 °C. The coercivity value increased with increasing grain size until critical grain size was reached. Crack-free films obtained in this work with a high value of saturation magnetization can be used in many applications.

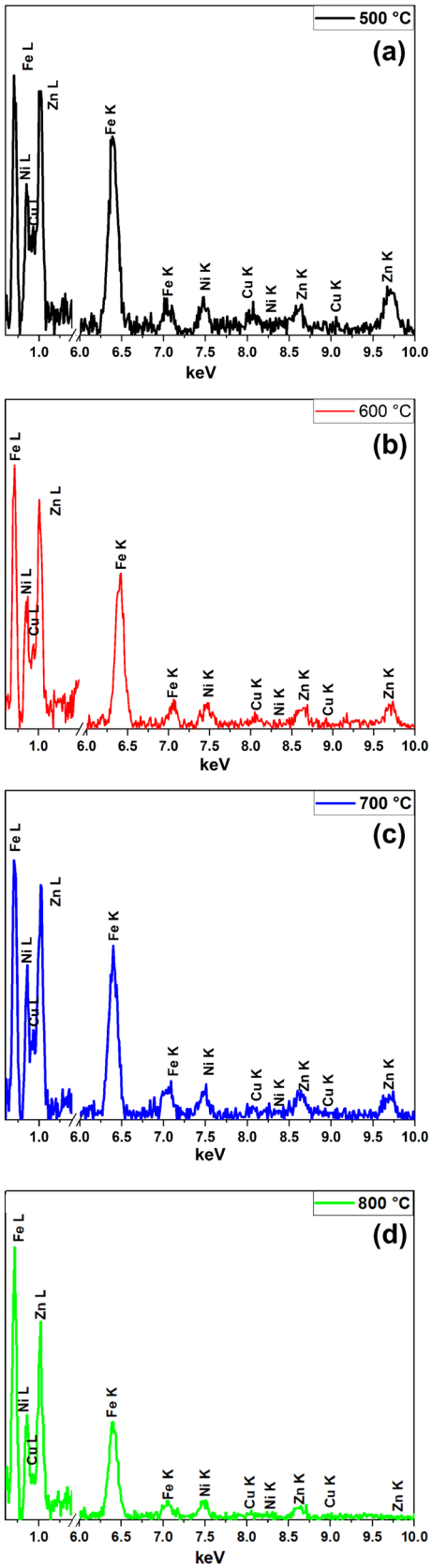

◀**Fig. 4** EDS spectrum of NCuZF films annealed at different temperatures: **a** 500, **b** 600, **c** 700, and **d** 800 °C

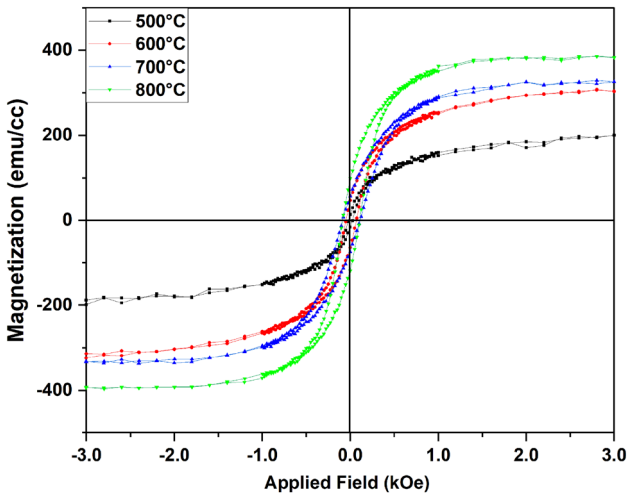

Fig. 5 Magnetization as a function of applied field for NCuZF films annealed at 500, 600, 700, and 800 °C

Acknowledgements

This work utilized resources owned and maintained by the Alabama Analytical Research Facility, which is supported by The University of Alabama. The authors acknowledge the Magnetic Materials and Device Laboratory at the University of Alabama for providing access to sputtering system.

Author Contributions

RP contributed to data collection, investigation, formal analysis, and visualization, and co-writing original draft; SK contributed to conceptualization, visualization, co-writing original draft, review & editing, funding acquisition, project administration, supervision, and resources; and JAAQ contributed to formal analysis, review & editing, funding acquisition, project administration, and resources.

Funding

This material is based upon work supported in part by the National Science Foundation under Grant No. 1708690. Any opinions, findings, and conclusions or recommendations expressed in this material are those

of the author(s) and do not necessarily reflect the views of the National Science Foundation.

Data availability

The datasets generated during and/or analyzed during the current study are available from the corresponding author on reasonable request.

Declarations

Conflict of interest The authors declare that they have no conflict of interest with the work submitted.

References

1. X. Luo, Y. Ma, B. Shao, C. Li, K. Li, D. Guo, D. Chen, H. Zhou, J Alloys Compd. **917**, 165380 (2022)
2. Y. Zheng, L. Jia, F. Xu, G. Wang, X. Shi, H. Zhang, Ceram. Int. **45**, 22163 (2019)
3. Y. Yang, J. Li, H. Zhang, J. Li, F. Xu, G. Wang, F. Gao, H. Su, Ceram. Int. **48**, 12490 (2022)
4. S. Yan, W. Liu, Z. Chen, Y. Nie, X. Wang, Z. Feng, J. Appl. Phys. **115**, 8 (2014)
5. Z.G. Yue, L. Li, J. Zhou, H. Zhang, Z. Ma, Z. Gui, Mater. Lett. **44**, 279 (2000)
6. A.A. Gaikwad, S.B. Kulkarni, J. Supercond. Nov. Magn. **34**, 2405 (2021)
7. T. Kagotani, R. Kobayashi, S. Sugimoto, K. Inomata, K. Okayama, J. Akedo, J. Magn. Magn. Mater. **290–291**, 1442 (2005)
8. F. Liu, T. Ren, C. Yang, L. Liu, A.Z. Wang, J. Yu, Mater. Lett. **60**, 1403 (2006)
9. J. Lee, Y.K. Hong, S. Bae, J. Jalli, J. Park, G.S. Abo, G.W. Donohoe, B.C. Choi, IEEE Trans. Magn. **47**, 304 (2011)
10. F. Xu, D. Zhang, Y. Liao, H. Zhang, Ceram. Int. **45**, 6350 (2019)
11. F. Li, S. Ye, S. Li, and X. Shi, NEMS 2011—6th IEEE International Conference on Nano/Micro Engineered and Molecular Systems **559** (2011)
12. F. Liu, C. Yang, T. Ren, A.Z. Wang, J. Yu, L. Liu, J. Magn. Magn. Mater. **309**, 75 (2007)
13. L.Q. Gao, G.J. Yu, Y. Wang, F.L. Wei, Chin. Phys. B **20**, 027503 (2011)
14. J. Li, Z. Yu, K. Sun, X. Jiang, Z. Xu, Z. Lan, J. Alloys Compd. **513**, 606 (2012)
15. Y. Liu, Y. Li, H. Zhang, D. Chen, C. Mu, J. Appl. Phys. **109**, 6 (2011)
16. S. Kotru, R. Paul, J.A. Abu Qahouq, Mater. Chem. Phys. **276**, 125357 (2022)
17. K. Sun, Y. Dai, Y. Yang, Z. Yu, H. Liu, X. Jiang, Z. Lan, Ceram. Int. **42**, 3028 (2016)
18. Y. Hong, I. de Moraes, G.G. Eslava, S. Grenier, E. Bellet-Amalric, A. Dias, M. Bonfim, L. Ranno, T. Devillers, N.M. Dempsey, J. Market. Res. **18**, 1245 (2022)
19. S.K. Choi, J.I. Lee, J. Vacuum Sci. Technol. A Vacuum Surf. Films **19**, 2043 (2001)
20. H. Xu, W. Zhang, B. Peng, W. Zhang, Appl. Surf. Sci. **257**, 2689 (2011)
21. X. Zuo, A. Yang, S.D. Yoon, J.A. Christodoulides, V.G. Harris, C. Vittoria, Appl. Phys. Lett. **87**, 1 (2005)
22. S.D. Yoon, C. Vittoria, S.A. Oliver, J. Appl. Phys. **92**, 6733 (2002)
23. C. Zhou, T. Li, X. Wei, B. Yan, Metals (Basel) **10**, 1 (2020)
24. K. Wang, Y. Huang, Z. Xu, S. Dong, R. Chen, J. Magn. Magn. Mater. **424**, 89 (2017)
25. L. Wu, C. Dong, X. Wang, J. Li, M. Li, J. Alloys Compd. **779**, 794 (2019)
26. A.R. Chavan, R.R. Chilwar, P.B. Kharat, K.M. Jadhav, J. Supercond. Nov. Magn. **31**, 2949 (2018)
27. K. Sun, Z. Lan, Z. Yu, X. Nie, L. Li, X. Zhao, J. Mater. Sci. **44**, 4348 (2009)
28. A. Sutka, R. Pärna, G. Mezinskis, V. Kisand, Sens. Actuators. B Chem. **192**, 173 (2014)
29. J. Xiang, X. Shen, F. Song, M. Liu, J. Solid State Chem. **183**, 1239 (2010)
30. A. Monshi, M.R. Foroughi, M.R. Monshi, World J. Nano Sci. Eng. **02**, 154 (2012)
31. M. Dongol, A. El-Denglawey, M.S. Abd El Sadek, I.S. Yahia, Optik (Stuttg) **126**, 1352 (2015)
32. A. Begum, A. Hussain, A. Rahman, Beilstein J. Nanotechnol. **3**, 438 (2012)
33. G.K. Williamson, R.E. Smallman, Phil. Mag. **1**, 34 (1956)
34. C. Rath, S. Anand, R.P. Das, K.K. Sahu, S.D. Kulkarni, S.K. Date, N.C. Mishra, J. Appl. Phys. **91**, 2211 (2002)
35. R. Kancharla and A. Vudayagiri, J Supercond Nov Magn (2022)
36. S. Regmi, Z. Li, A. Srivastava, R. Mahat, K.C. Shambhu, A. Rastogi, Z. Galazka, R. Datta, T. Mewes, A. Gupta, Appl. Phys. Lett. (2021). https://doi.org/10.1063/5.0047865
37. D.K. Pradhan, S. Kumari, D.K. Pradhan, A. Kumar, R.S. Katiyar, R.E. Cohen, J. Alloys Compd. **766**, 1074 (2018)
38. M.C. Dimri, A. Verma, S.C. Kashyap, D.C. Dube, O.P. Thakur, C. Prakash, Mater. Sci. Eng. B Solid State Mater. Adv. Technol. **133**, 42 (2006)
39. L.S. Wang, S.J. Nie, J.B. Wang, L. Xu, B.B. Yuan, X.L. Liu, Q. Luo, Y. Chen, G.H. Yue, D.L. Peng, Mater. Chem. Phys. **160**, 321 (2015)

40. R.K. Singh, C. Upadhyay, S. Layek, A. Yadav, Int. J. Eng. Sci. Technol. **2**, 104 (2010)
41. D.S. Mathew, R.S. Juang, Chem. Eng. J. **129**, 51 (2007)
42. M. Bissannagari, J. Kim, Ceram. Int. **41**, 8023 (2015)